J Digit Imaging (2013) 26:129–139
DOI 10.1007/s10278-012-9481-7

Segmentation of the Common Carotid Artery Walls Based on a Frequency Implementation of Active Contours

Segmentation of the Common Carotid Artery Walls

M Consuelo Bastida-Jumilla · Rosa M Menchón-Lara · Juan Morales-Sánchez · Rafael Verdú-Monedero · Jorge Larrey-Ruiz · José Luis Sancho-Gómez

Published online: 3 May 2012

Abstract Atherosclerosis is one of the most extended cardiovascular diseases nowadays. Although it may be unnoticed during years, it also may suddenly trigger severe illnesses such as stroke, embolisms or ischemia. Therefore, an early detection of atherosclerosis can prevent adult population from suffering more serious pathologies. The intima–media thickness (IMT) of the common carotid artery (CCA) has been used as an early and reliable indicator of atherosclerosis for years. The IMT is manually computed from ultrasound images, a process that can be repeated as many times as necessary (over different ultrasound images of the same patient), but also prone to errors. With the aim to reduce the inter-observer variability and the subjectivity of the measurement, a fully automatic computer-based method based on ultrasound image processing and a frequency-domain implementation of active contours is proposed. The images used in this work were obtained with the same ultrasound scanner (Philips iU22 Ultrasound System) but with different spatial resolutions. The proposed solution does not extract only the IMT but also the CCA diameter, which is not as relevant as the IMT to predict future atherosclerosis evolution but it is a statistically interesting piece of information for the doctors to determine the cardiovascular risk. The results of the proposed method have been validated by doctors, and these results are visually and numerically satisfactory when considering the medical measurements as *ground truth*, with a maximum deviation of only 3.4 pixels (0.0248 mm) for IMT.

Keywords Automated measurement · Image segmentation · Ultrasound · Intima–media thickness

M. C. Bastida-Jumilla (✉) · R. M. Menchón-Lara · J. Morales-Sánchez · R. Verdú-Monedero · J. Larrey-Ruiz · J. L. Sancho-Gómez
Tecnologías de la Información y las Comunicaciones Department, Universidad Politécnica de Cartagena,
Campus Muralla del Mar, Antiguo Cuartel de Antigones, s/n,
30202 Cartagena, Spain
e-mail: consuelo.bastida@upct.es

R. M. Menchón-Lara
e-mail: rmml@alu.upct.es

J. Morales-Sánchez
e-mail: juan.morales@upct.es

R. Verdú-Monedero
e-mail: rafael.verdu@upct.es

J. Larrey-Ruiz
e-mail: jorge.larrey@upct.es

J. L. Sancho-Gómez
e-mail: josel.sancho@upct.es

Introduction

Atherosclerosis consists of a thickening of the arterial walls. Although it is very spread into population and it may trigger strokes, embolisms or ischemia, it could be unnoticed for years. Therefore, medical research has been focusing on early detection of atherosclerosis. The intima–media thickness (IMT) has emerged as an early and reliable indicator of atherosclerosis [1], making the tracking of the IMT possible with the aim of avoiding the worsening of atherosclerosis and cardiovascular risk.

Another factor to take into account is that the IMT measurement is extracted by means of a B-mode ultrasound scan. Since it is a non-invasive technique, the IMT measurement facilitates studies over a large population.

The use of different protocols to measure the IMT [2] and the variability between observers is a recurrent problem of the manual measurement procedure. Therefore, the

establishment of a single protocol to measure the IMT presents an important challenge. Nowadays, IMT is considered as a reliable indicator of atherosclerosis when the measurement protocol presents repeatability and reproducibility [3, 4]. In particular, the processing proposed is intended to take advantages of a methodical acquisition protocol [2], whose authors (from the Radiology Department from Hospital Universitario Virgen de la Arrixaca (Murcia, Spain)) have provided all the images used. The radiologist takes from one to three point pairs on the far (posterior) wall of the vessel along a 1-cm-long section proximal to the bifurcation. The measurement corresponding to the maximum IMT is recorded.

The pictures were obtained with the ultrasound scanner Philips iU22 Ultrasound System, following the process described in [2]. Even though using the same transducer, the spatial resolution of the images varies from one to another, ranging from 0.029 to 0.067 mm/pixel. In other words, the radiologists use always the same probe, but it is their choice to change the image zoom or not.

The manual procedure consists of marking a pair of points that delimits the IMT over a longitudinal cut of the CCA, around 1 cm after its bifurcation. On the image in Fig. 1, an example of the manual procedure is shown, where the interfaces between the lumen, where the blood flows, and the near (at the top of the image) and far (at the bottom) walls can be seen. At the far wall, a typical bright–dark–bright pattern can be appreciated. This pattern corresponds to the intima–media–adventitia layers of the arterial walls. The IMT is defined as the distance between the lumen–intima interface (I5) and the media–adventitia interface (I7), which is measured by means of two points (one on each interface) marked by the doctor, whereas through the segmentation of the interfaces I5 and I7 two lines would be obtained. As a result, not only would the IMT be measured more precisely but also other interesting statistics could be calculated along the artery length, such as mean, median or maximum IMT.

Besides, the use of ultrasound image processing to extract IMT would increase reproducibility, avoid subjectivity and, since it is a non-invasive technique, it would also allow the automatic analysis of a large amount of images. The preceding idea makes the IMT automatic detection of great interest to make studies over a large population.

Background

With the use of IMT as a cardiovascular risk indicator, there have been several attempts to improve its measurement procedure by making it user independent. Since the work of Gustavsson et al. [5], different image processing methods have appeared. Most of them were based on an analysis of vertical cuts of the image [5, 6], on active contours [7, 8] or on a combination of both [9].

Methods based on the analysis of the characteristics of vertical cuts of the image determine the boundary location by taking into account local information. Many of them included a cost function to minimize in order to introduce a continuity term to avoid irregular borders. Despite the use of a continuity term, the data are still locally derived. Moreover, none of them was completely automatic; they required user interaction, even though it consisted on giving only two points nearby the arterial wall or the horizontal seek position [5]. Those based on active contours avoid the locality problem but, since initialization is critical for active contours [10], the aforementioned works (amongst others) include user interaction to initialize the contours.

The combination of both concepts (active contours and vertical analysis of the image) can even require some user interaction, except for the proposals of Molinari et al. [11–13]. Up to our knowledge, fully automatic methods cannot be found in the literature until the publication of the work of Molinari et al. However, these methods (including Molinari et al.) do not deal with different spatial resolutions;

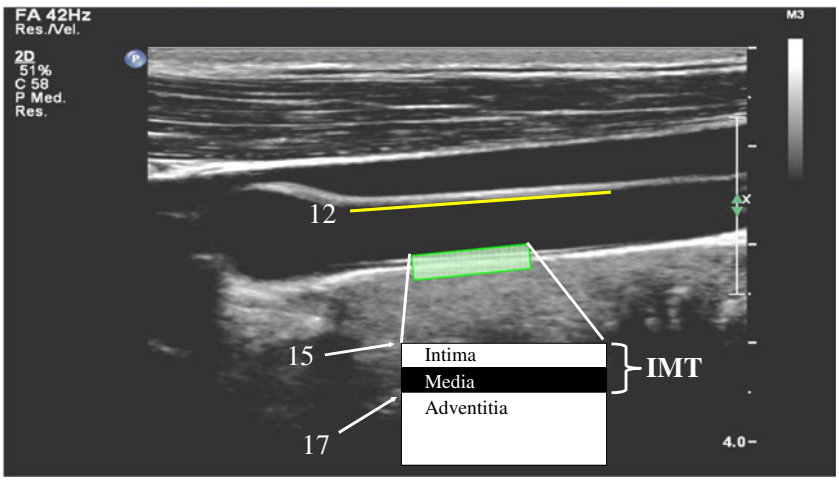

Fig. 1 Interfaces to be detected and IMT over an example ultrasound image

the images they use present always the same zoom level or equivalence pixel to millimetres, which simplifies the wall detection. Moreover, they present some problems in the presence of blood turbulences or hard carotid plaques, and they do not segment the near wall. In our case, we pretend to obtain a fully automatic method, with an edge detection based on active contours which delimits near wall (I2) as well as extracts IMT.

CCA Segmentation Process

The process followed to delimit the intima and adventitia layers of the CCA and the near wall is shown in Fig. 2. Firstly, the input parameters of the interfaces delimitation process, the initial contours and the driving forces of the image, are calculated. The detection of the interfaces I2, I5 and I7 is controlled by an active contour algorithm. After the detection, the validity of the measurements is assessed. If the measurements are correct along all the artery length, the process ends. Otherwise, a refinement process takes place to improve the results.

This refinement step affects only the far wall, mainly because the near wall edge appears clearer and it is highly likely that the algorithm reaches the final solution in the layer detection stage. By not taking the near wall contour into account, the computational cost of the second stage is considerably reduced. Besides, the initial contours for intima and adventitia layers are pretty close to the final solution, requiring, thus, of very few iterations.

Since one of the critical issues in active contour algorithms, additionally to the local minima and the reduced convergence speed in concave regions, is the initialization of the contours [10], a great effort has been made to obtain appropriate initial contours. This is the reason why the step of automatic initialization (see "Automatic Initialization" section) is the most elaborated in our process. In the sections below, each of the steps shown in Fig. 2 will be explained.

Wall Detection

Automatic Initialization

In the flow chart shown in Fig. 3, the followed steps to calculate the initial contours are shown. In the next sections, a description of each of the processing stages will be detailed.

CCA Angle Correction Although most of the images present only a slight inclination, the CCA angle with respect to the horizontal direction is calculated to easily detect the position of the far wall. As a previous step to the angle correction, the image is cropped to make the image anonymous and to consider only the anatomical information on the ecography. The crop size is fixed and the same for all the images. Over this cropped image, a horizontal Sobel operator [14] is applied to detect the horizontal edges of the artery. After that, the main direction of the artery is detected by computing the Hough transform [15] of the edges. This orientation will give us the CCA angle, which can be corrected by rotating the cropped image. A bilinear spatial interpolation has been used in the rotation because it gives the best trade-off between computational cost and image quality [14].

Far Wall Detection The next step to obtain an automatic initialization (see Fig. 3) is to determine the location of the far wall (see flow chart in Fig. 4). Correlation of the cropped image with a model is used for this purpose. Since we want

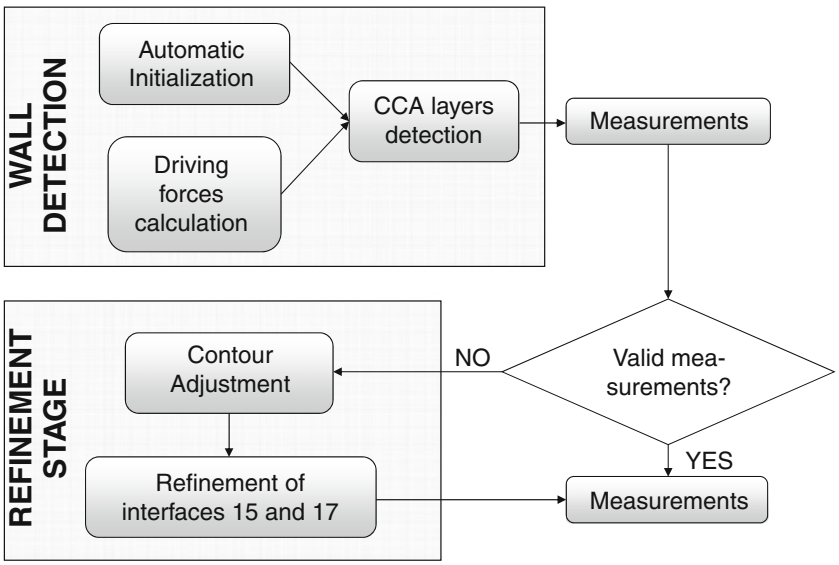

Fig. 2 Flow chart of the CCA processing

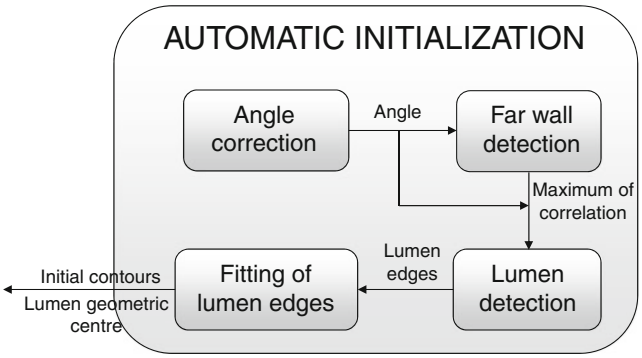

Fig. 3 Automatic initialization diagram

to locate the far wall, the model must contain a portion of it. The model was extracted from a generic ultrasound image of the CCA. To improve the correlation results, the model must present a clear light–dark–light interfaces pattern (corresponding to the far wall), should be small to reduce computational cost and must produce good correlation outcomes with most of the considered images. To fulfil the latter, a smoothing has been applied to the model.

Since correlation is not reliable in the extremes [14] and the CCA is usually centred in the cropped image, the image has been vertically weighed so that the pixels near to the top and the bottom limits are weakened. After that, only the pixels with intensity above a threshold of 0.2 in the range [0, 1] are taken into account. This threshold has been chosen after multiple tests because it guaranteed to detect far and near wall separately and minimized the number of false positives.

The different resulting regions are isolated and their areas are measured. The two regions with the largest areas correspond to the near and far wall regions. Afterwards, we check that the point of maximum correlation is located between these two regions. Otherwise, the maximum and its neighbouring pixels are discarded and the following maximum correlation position is considered. This process repeats until a valid maximum (i.e. a maximum located between the near and far walls of the CCA) is found. This point will be used as input data in the following steps (see Fig. 3).

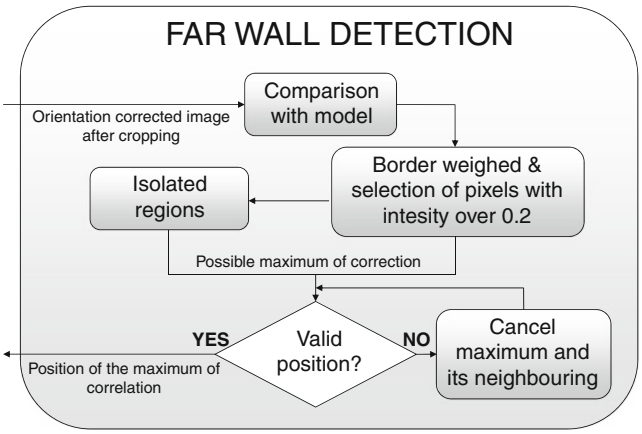

Fig. 4 Far wall detection flow chart

Lumen Detection A median filtering is used to detect the dark area corresponding to the lumen. To optimize the filtering output, the inclination of the CCA is corrected over the image (see flow chart in Fig. 5) and a horizontally oriented filter is used. The median filtering is iteratively applied to the image with the artery in horizontal position to reduce speckle noise influence. By doing this, the image is slightly blurred while maintaining its edges [14], achieving smooth homogeneous regions.

Later, the image is binarized and its negative is taken to obtain a binary image with several white regions, one of them corresponding to the lumen. After filling possible holes, the region which contains the point of maximal correlation will be selected as lumen, resulting in a binary mask of the lumen.

Initial Contours Calculation Once the lumen edges have been detected, a polynomial interpolation of order 3 is applied to them to obtain smoother initial contours corresponding to the near and far wall of the CCA. The lower contour is split into two, one to detect the intima and another to detect the adventitia layer. Both curves are slightly displaced with respect to their original position. In particular, the upper contour (corresponding to the intima layer) is moved 15 pixels upwards, while the lower (corresponding to the adventitia layer) is placed 35 pixels under the previous one.

At this point, it is possible to calculate the position of the "geometric centre" of the lumen, which will be employed in later processing. The geometric centre is calculated as the mean point from the lumen region. Especially the vertical coordinate position of the geometric centre is of our interest, since it establishes a clear reference point between near and far walls (see Fig. 7c).

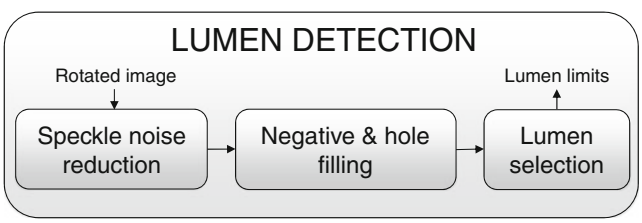

Fig. 5 Lumen detection process

Driving Force Calculation

Driving forces, extracted from the cropped original image, control where the contours adjust. Usually, the gradient or Laplacian of the image values are used as driving forces, since they show the position of intensity transitions where the layer boundaries are located. The calculation process to determine drive forces is shown in Fig. 6. In the cropped image (the crop is the same used in previous sections), pixels with low intensity are forced to 0 to eliminate its influence in the calculation of the gradient.

After that, a low-pass Gaussian filter is applied to smooth the edges. Since the artery presents a nearly horizontal inclination, the intensity changes we are interested in are those which occur in the vertical direction. Thus, only the gradient in the vertical direction is calculated. However, the desired transitions are different for each wall. Namely, for the near wall, the required transition is decreasing (from light to dark, see Fig. 7a) and for the far wall is increasing (from dark to light, see Fig. 7b). Given that the geometric centre of the lumen delimits the border where the wanted transitions change from decreasing to increasing, the combination of both types of transition is possible, as can be seen in Fig. 7c.

To slightly eliminate some noise (see Fig. 6), a morphological filtering is performed. Morphological filtering allows us to find elements in the image with similar morphology as the so-called structuring element [14]. More specifically, a closing (to join unconnected regions) and an opening (to eliminate small regions) with horizontally oriented structuring element has been applied (see Fig. 8a).

The following step is to find the main three directions in the image; a Hough transform is used. The Hough transform [15] estimates the main geometric orientation of the structures in the image. In our case, we extract via a Hough transform the main three directions in the image, which will give us a morphological mask (see Fig. 8b) to reconstruct the gradient image with reduced noise. Now, having eliminated the information with different orientation from the main three directions in the image, the resulting image is clear and visually less noisy (see Fig. 8c). Finally, a gradient operation over this image is computed to get the forces which will drive the active contour algorithm.

CCA Layer Detection

As explained at the very beginning of "CCA Segmentation Process" section, the process to detect interfaces I2, I5 and I7 is determined by an active contour algorithm, which presents an iterative evolution as can be inferred from Fig. 9. There will be three contours, one for each interface to detect.

The process starts with an interpolation over the initial curves calculated in "Automatic Initialization" section. By interpolating, the different points or nodes u that comprises the contours are linked with a shape function that determines extra points between the nodes called "control points" v. Cubic B-splines are used as shape function because they produce smooth contours, avoid the influence of the characteristic rough texture in ultrasound images and provide the best performance regarding its computational load. By introducing this interpolation, the number of calculations considerably decreases because only a few nodes affect the snake evolution. Besides, a frequency-domain formulation of the image processing algorithm has been employed [16], which offers substantial computational savings in comparison to the time-domain formulation, especially for two-dimensional structures [17].

After the node interpolation, the Laplacian affecting each control point is evaluated. The Laplacian value, acting as external force, is applied over the nodes together with the gravity and take-off forces. These latter forces act mainly in the first iterations if the contour does not reach any edge, i.e. if the contour location coincides with a gradient value of zero. In that case, curves for I2 and I7 will be affected by take-off forces that push them upwards, whereas I5 curve will be forced downwards by the effect of gravity forces.

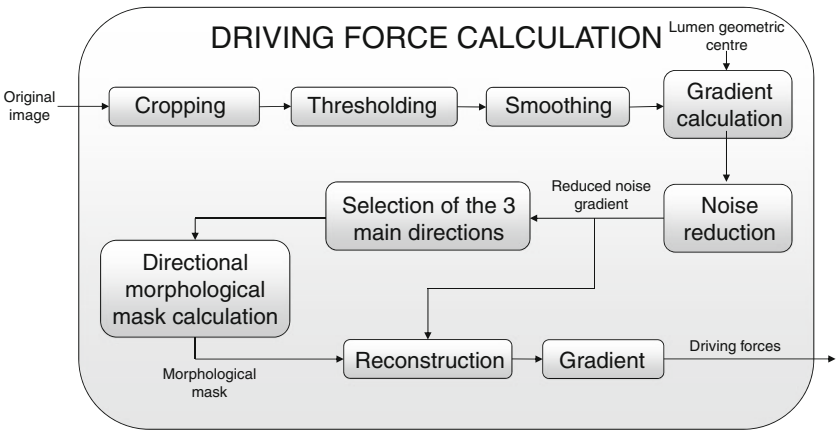

Fig. 6 Driving forces calculation diagram

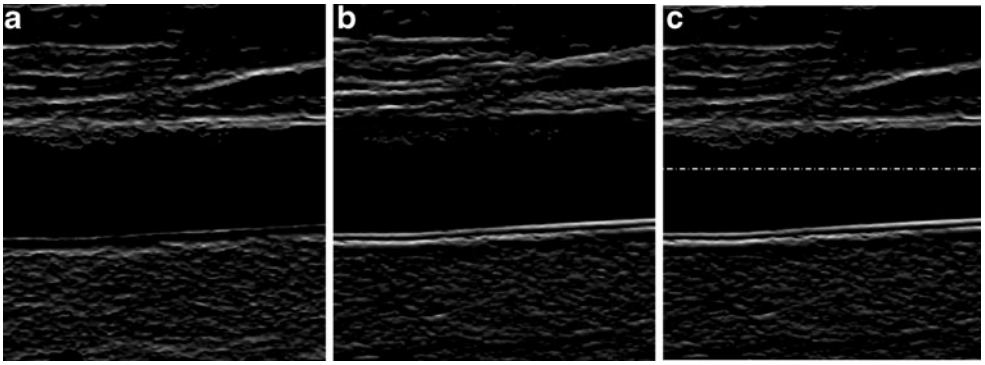

Fig. 7 Combination of decreasing (**a**) and increasing (**b**) gradient transitions in a single image (**c**) from image #14. The *dotted line* marks the border between near and far wall

When all the forces affecting the nodes are calculated, the position of the nodes in the next iteration is obtained, always forcing far wall curves not to cross. Finally, the process will continue until the end condition is reached. This condition involves two requirements; on the one hand, the combined movement of curves I5 and I7 must be less than 0.1 pixel (less than 0.017 % of the vertical size). On the other hand, the displacement in the next iteration for I2 must be less than 0.05 pixel, which implies a displacement of 0.085 % of the vertical size of the image. If one of the conditions is fulfilled, the corresponding contour evolution will stop. If neither of the conditions is reached, the algorithm will stop after 1,000 iterations, which are sufficient for the curves to converge in all cases.

Measurements and Validation

Before extracting measurements, it is necessary that the contours are placed near an edge and that they present continuity. To accomplish that, we focus on finding the bimodal profile with two intensity peaks that must appear in the vertical cuts of the image.

To make the search of a bimodal profile simpler, the histogram of the distance between the far wall contours (I5 minus I7) is considered. Hence, the difference of a bimodal distribution will produce a Gaussian distribution. However, if the difference shows some outliers (IMT too big or too small with respect to the most repeated values), we consider that the outlier was produced because of an inadequate wall detection, such as in the case of image #16 (see Fig. 10a).

To eliminate the aforementioned outliers, a Gaussian window is applied to the histogram of the difference (Fig. 10b). The window weighs the values in the histogram by multiplying them with a Gaussian function. Since a health adult's CCA presents usually IMT from 0.05 cm, the mean of the window is the median IMT over the values above 6 pixels (equivalent to less than 0.44 mm for the maximum space resolution) and the standard deviation is 1 pixel (0.079 mm for the maximum space resolution). By doing this, the values of IMT too small are discarded. After multiplying by the Gaussian window, all the bins under 1 % of the most repeated IMT value are discarded. With this method, the limits where the IMT measurement has been validated are established, as can be seen in Fig.10c, where the dotted line indicates non-validated measurement and the continuous one valid measurement. This "IMT range" will be used in later processing. Over the IMT range, some variation margin is allowed depending on the number of values discarded with the Gaussian window. The more discarded values, the greater variation with respect to the original range the "expanded range" will admit. In the case of image #16 (see Fig. 10a, b), the IMT range ranges from 8 to 16 pixels (0.266 to 0.532 mm), and the expanded range varies from 10 to 21 pixels (0.332 to 0.698 mm).

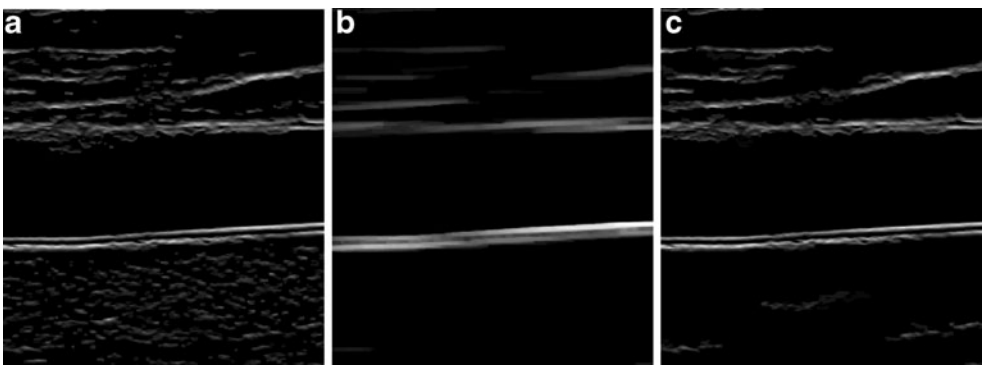

Fig. 8 Gradient from image #14 with reduced noise (**a**), directional morphological mask (**b**) and gradient reconstruction with the directional mask (**c**)

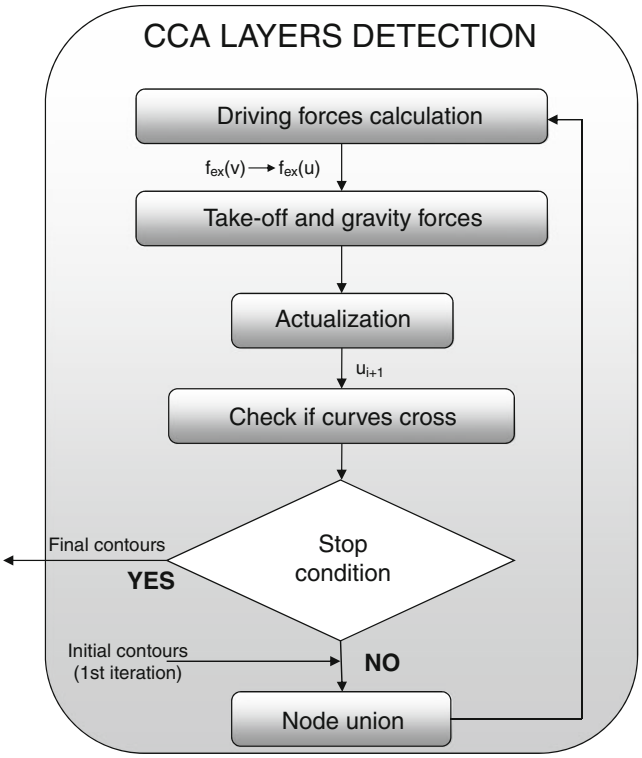

Fig. 9 Flow chart of the iterative active contour process

Refinement Stage

Contour Adjustment

If there are non-validated sections in the solution found (as shown in Fig. 10c), the contours corresponding to interfaces I5 and I7 must be properly reinitialized, but only in those sections considered as non-validated (see Fig. 11). These validated sections will be trimmed five control points *v* on each side to avoid that the validated contours with short extension have a significant weight in the adjustment.

Usually, for each non-validated section, only one contour converges to a wrong solution, forcing us to reconsider the traced contours. For this purpose, the wrong (or perhaps the worse) contour in each non-validated section is determined. The contour with the higher curvature in a non-validated section will be considered the wrong curve in that specific section. The followed criterion to establish which curve is wrong is based on the second spatial derivative. Thus, the curve with the bigger absolute value of its second derivative in the non-validated section will be considered as the wrong curve.

The previous process is repeated for all the non-validated sections to proceed with a low-order interpolation (2 or 1 if the value of the measured curvature is too small) over the wrong sections. The interpolation takes as known points those of the validated sections, making an estimation of the non-validated sections. If the new contours twist or if they separate further than the "expanded IMT range", they are force to keep a distance within the "expanded IMT range".

Since a non-validated measurement could be due to insufficient intensity or to the existence of an attracting nearby edge (driving force), together with this adjustment, the gradient for each contour is weighed. In other words, the intensity of the external forces in areas far from the new initialization is reduced. For this purpose, a Gaussian function with 40 pixels wide (6.77 % of the image height) and standard deviation 35 pixels (around 6 % of the image height) centred in the new contour position is applied. As a consequence, nearby edges lose intensity to avoid the contours reaching them. This is again the case for image #16, which is shown in Fig. 12.

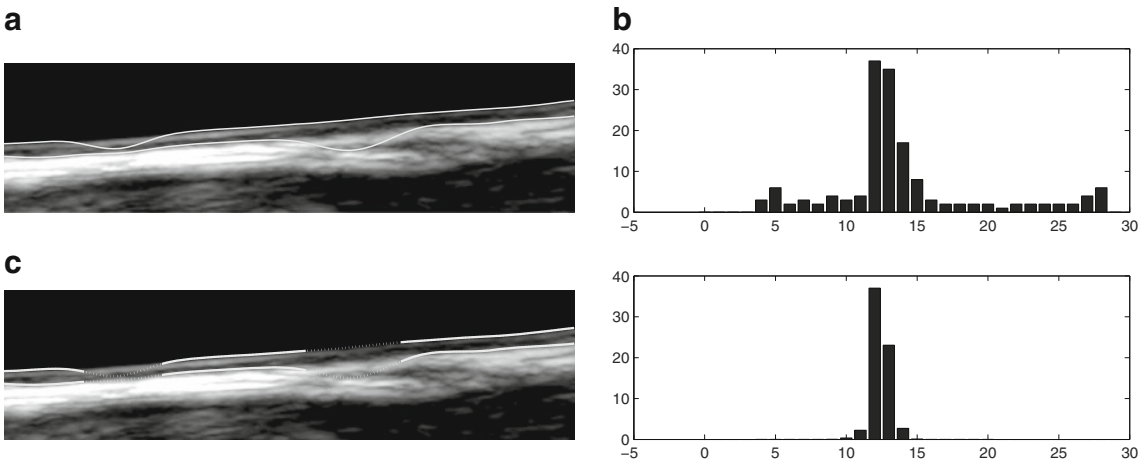

Fig. 10 Wall detection results for image #16 (**a**), measurement validation histograms before (*top*) and after (*bottom*) the application of a Gaussian filter (**b**) and validated results (**c**)

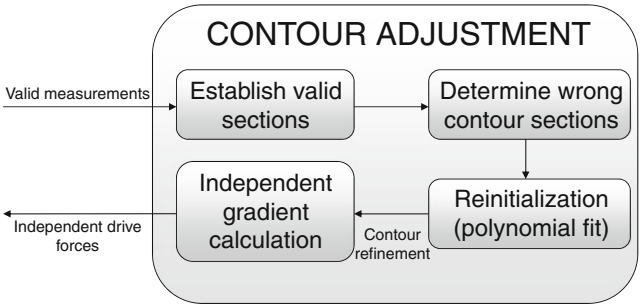

Fig. 11 Contour adjustment process previous to the refinement stage

Refinement of Interfaces I5 and I7

In the results refinement stage, the processing is very similar to that explained in "CCA Layer Detection" section (see Fig. 9). The basic differences lie in the fact that only contours corresponding to interfaces I5 and I7 will evolve and that each one has a different driving forces. As an example, results after the first stage for image #16 are shown in Fig. 12a, where the first wrong section is due to the upper contour and the second wrong section to the lower one. Therefore, a different gradient image is applied to the curves I5 (see Fig. 12b) and I7 (see Fig. 12c), respectively.

Measurements and Validation After Refinement

After the results refinement, the validation criterion is different from that used in "Measurements and Validation" section. Now, valid IMT measurements must lie over intensity peaks. This was not previously considered because it could cause results like those in Fig. 10a. In other words, the existence of intensity peaks under the obtained contours did not initially guarantee that the bimodal profile was the desired one. However, after the refinement process, the intensity peaks can be considered as suitable locations for the final contours.

Following this idea, intensity peaks are sought using a classical K-means method with two classes, extracting a binary image from the gradient of the image used as external force. The nodes are then moved to the intensity peaks found via K-means.

Finally, to assure the final contours smoothness, a last checking is made. An order 2 polynomial fit is calculated over the contours obtained in the previous section. If the maximum difference between the non-validated section position and the polynomial fit is less than 3.5 pixels (0.256 mm for the maximal vertical space resolution), that section will be definitely considered as valid. By doing this, a smoothness criterion is established, considering valid sections where there is no information but where that IMT value is to be expected with enough guarantees. It is also possible that the intensity peak be too weak and then, even though it may be the desired position, it be considered as non-validated. Figure 13 illustrates this situation.

Results

The provided images can be classified into three different datasets. One contains images with overlaid markers placed by the doctors, another one shows raw images (i.e. images without any overlapped element) and the third one contain the same images with and without markers for a better comparison between manual procedure and our method.

In Fig. 14, the obtained results for different images can be seen over the images marked by the doctors. Under each image, the mean relative error and the mean difference in millimetres are shown. Taking into account all the marked and validated locations, the mean relative error has been calculated as the averaging of the relative deviations of the algorithm measurement with regard to the doctor's ones. For this dataset, the relative error remains under 3.25 %. We found the maximum deviation in pixels for the marker at the right in Fig. 14c, which is of only 2.2 pixels (0.0726 mm).

In Fig. 15, a second CCA image set is shown. These images do not have any overlaid markers, and their corresponding results have been only visually validated by the doctors. It is remarkable that although the case in Fig. 15b did not present the intima–media–adventitia pattern along all the length of the cropped image, the proposed method has achieved a good result and has correctly evaluated the validity of the final contours.

Finally, in Fig. 16, IMT measurements extracted from images without markers are compared to the quantitative measurements obtained by the doctors from the same images. Under each image, the mean relative error,

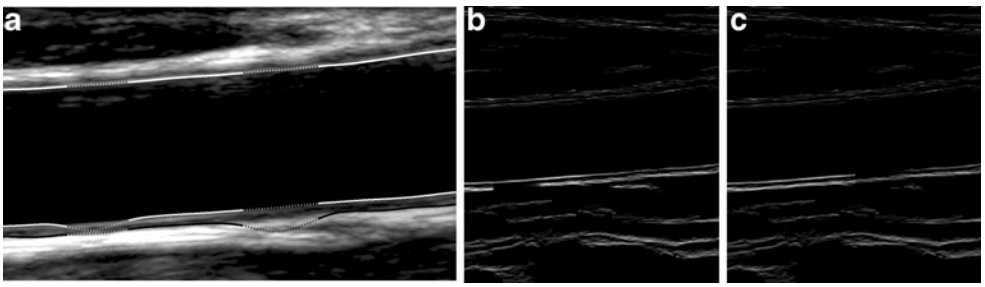

Fig. 12 Example of independent gradient images for image #16: **a** results after the first stage, **b** gradient for the upper and **c** lower contour in the refinement stage

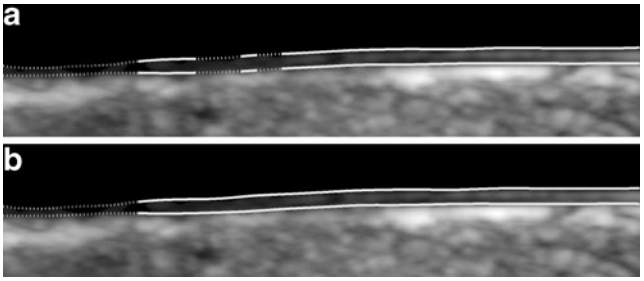

Fig. 13 Validation example for image #15. Before (**a**) and after polynomial fit (**b**)

calculated as explained at the beginning of the present section (along with the mean difference in millimetres), between the segmentation here presented and the medical measurements is displayed, but only for those markers located in a validated section. This difference is calculated only at those points where the doctor has placed a marker to properly compare both methods.

The image in Fig. 16a presents the maximum mean relative error (9.71 %). This is due to a deviation of 0.1056 mm (1.6 pixels) for each marker under a validated section. Although the difference in pixels is small, the dependence of the relative error on the spatial resolution produces a high error (9.71 %).

Visually, we can appreciate that the final contours reach the markers placed by the doctors or that they lie nearby, with a maximum deviation of 2.7 pixels for the left marker in Fig. 16b. Once more, this image presents a low spatial resolution (0.067 mm/pixel) in comparison with other images. Thus, a small difference in pixels could translate into a large difference in mm (0.1809 mm), which affects negatively to the mean error. For all the images, the relative error of the difference between the manual and the automatic measurement at the selected locations remains always under 10 %.

To improve the near wall segmentation, its detection should be independently validated (see Fig. 16b). By limiting the curvature of the correct final contour, we could determine a new incorrect section and exclude the invalid lumen diameter measurements from the mean, maximum and minimum measurements.

Conclusions

Thanks to the image processing techniques described along this work, both near and far walls are correctly located in the available ultrasound images. This allows the development of a fully automatic method, in which the user interaction is not necessary at all. Being the initialization critical issue in the active contour evolution, many efforts and computational cost have been invested in automatically obtaining appropriate initial contours. Apart from having a completely automatic initialization, the method here presented overcome previous methods based on snakes because it implements the contours in a frequency domain, which provide

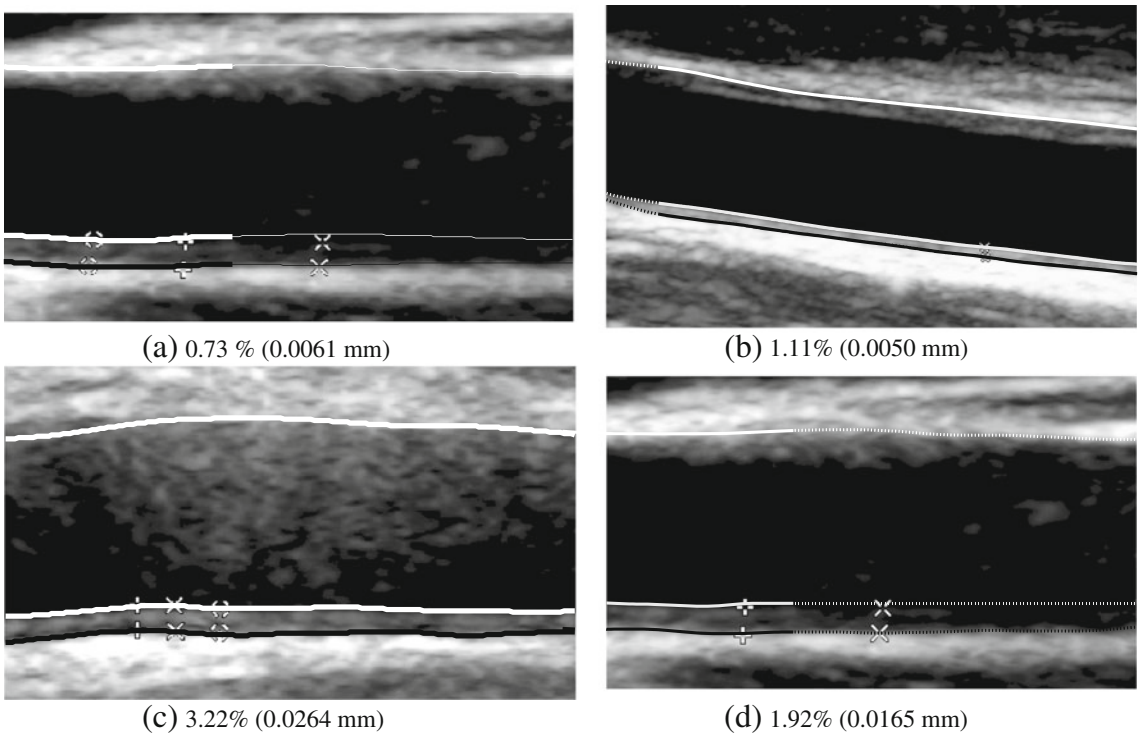

Fig. 14 Segmentation for images with markers and relative error in percentage (in millimetres)

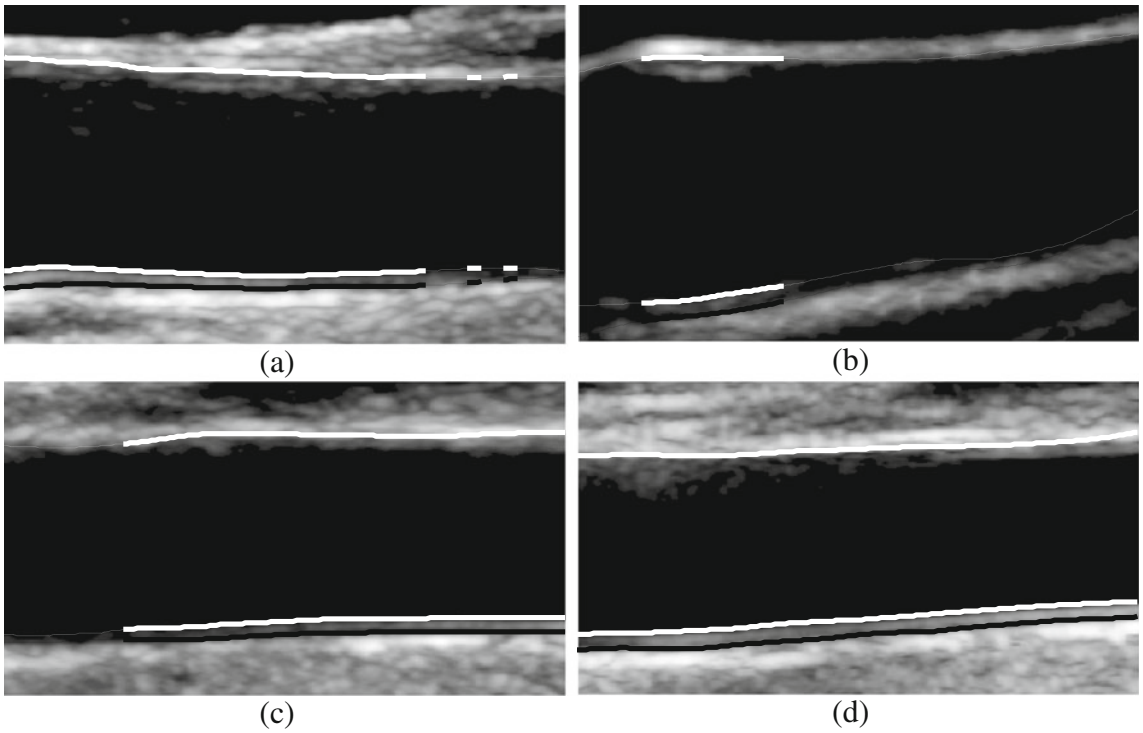

Fig. 15 Segmentation for images without markers

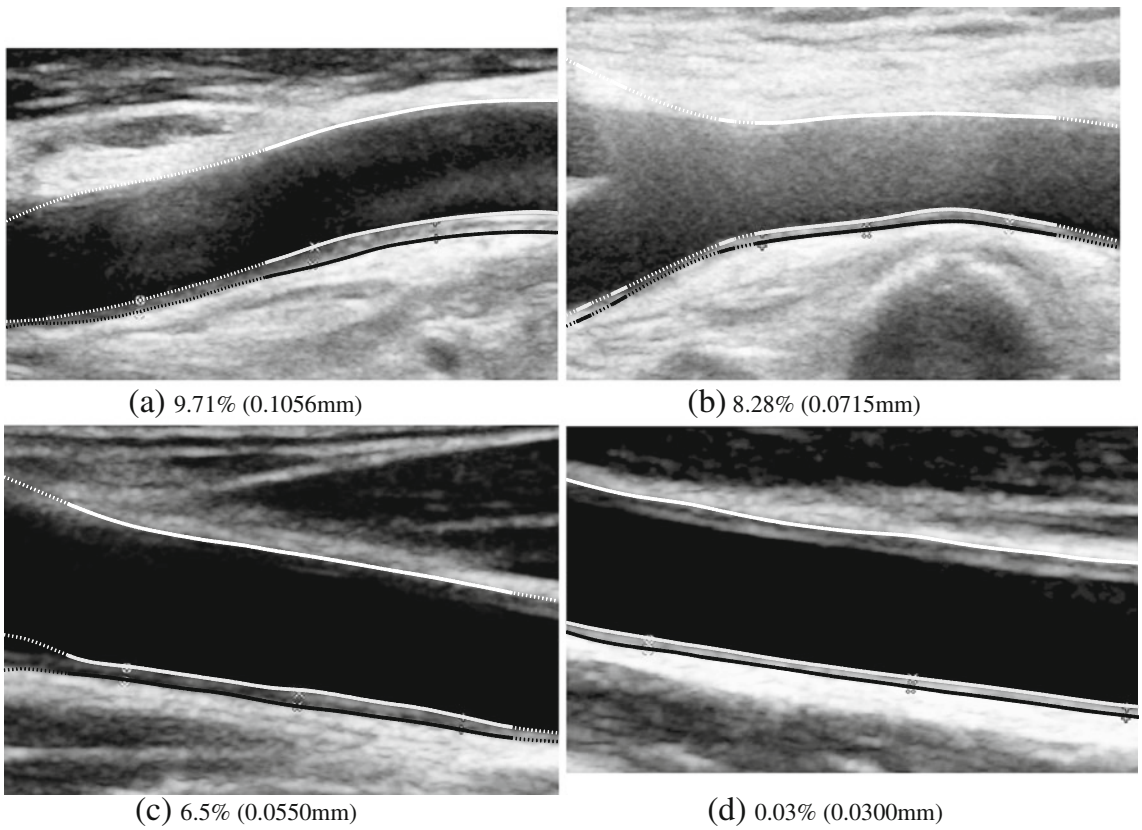

Fig. 16 Segmentation for images without markers over the images marked by the doctors and relative error in percentage (in millimetres)

significant computational savings (especially for two-dimensional structures) [16].

The shape function used in active contours is a cubic B-spline. This shape form has been chosen for its good performance versus running ratio and because it produce smooth edges [18]. Besides, the evolution of the contours divided into two stages requires short execution time than that in a single stage allowing more freedom to the curves because in the second stage the contours are initialized quite close to the final solution.

It is noteworthy that for both stages, the contours evolve simultaneously, reducing the running time when compared to previously published solutions [8], where the evolution of the curves for I5 and I7 is sequential. The validity of the results is studied based on statistical features after the CCA layer detection and on intensity features after the refinement process. This validation distinguishes correct from wrong sections of the final results, avoiding the inclusion of the latter in the statistical measurements. Apart from correctly assessing the results, this automatic validation can even help the doctors to decide where the most appropriate regions to measure IMT are.

The authors are studying how to mix both features (statistical and based on intensity) to merge both validation steps into a single one and to eliminate the second contour evolution stage, while maintaining the iteration reduction. In other words, the idea is to correct the non-validated sections after a single snake stage.

Both numerical and visual results have been endorsed by the doctors. The mayor discrepancies occur when the zoom level is too low (i.e. low spatial resolution), since a small difference in pixels translates into a high difference in millimetres. This result is to be expected because the less zoom, the worse the doctor can distinguish the interfaces to detect.

Authors are currently working on a comprehensive validation of the presented methodology, which includes many more images and medical measurements (concerning the IMT and the lumen diameter) for its comparison. At the moment, these results confirm those presented in this paper.

Acknowledgements This work is supported by the Spanish *Ministerio de Ciencia e Innovación*, under grant TEC2009-12675, and by the *Séneca* Foundation (09505/FPI/08). The authors would like to thank the Radiology Department of Hospital Universitario Virgen de la Arrixaca for their kind collaboration and for providing all the ultrasound images used.

References

1. Loizou CP, Pantziaris M, Pattichis MS, Kyriacou E, Pattichis CS: Ultrasound image texture analysis of the intima and media layers of the common carotid artery and its correlation with age and gender. Comput Med Imaging Graph 33(4):317–324, 2009
2. Velazquez F, Berná JD, Abellan JL, Serrano L, Escribano A, Canteras M: Reproducibility of sonographic measurements of carotid intima–media thickness. Acta Radiol 49(10):1162–1166, 2008
3. Gonzalez J, Wood JC, Dorey FJ, et al: Reproducibility of carotid intima–media thickness measurements in young adults. Radiology 247(2):465–471, 2008
4. Bots ML, Evans GW, Riley WA, Grobbee DE: Carotid intima–media thickness measurements in intervention studies: design options, progression rates, and sample size considerations: a point of view. Stroke 34:2985–2994, 2003
5. Gustavsson T, Liang Q, Wendelhag I, Wikstrand J: A dynamic programming procedure for automated ultrasonic measurement of the carotid artery. In: Proc. IEEE Comput Cardiol, 1994, pp 297–300
6. Liang Q, Wendelhag I, Wikstrand J, Gustavsson T: A multiscale dynamic programming procedure for boundary detection in ultrasonic artery images. IEEE Trans Med Imaging 19:127–142, 2000
7. Chan R, Kaufhold J, Hemphill LC, Lees RS, Karl WC: Anisotropic edge-preserving smoothing in carotid B-mode ultrasound for improved segmentation and intima–media thickness (IMT) measurement. Comput Cardiol 27:37–40, 2000
8. Ceccarelli M, De Luca N, Morganella A: An active contour approach to automatic detection of the intima–media thickness. In: IEEE International Conference on Acoustics, Speech and Signal Processing, ICASSP'06. doi:10.1109/ICASSP.2006.1660441, 2006
9. Loizou CP, Pattichis CS, Pantziaris M, Tyllis T, Nicolaides A: Snakes based segmentation of the common carotid artery intima media. Med Biol Eng Comput 45:35–49, 2007
10. Liang J, McInerney T, Terzopoulos D: United snakes. Med Image Anal 10(2):215–333, 2006
11. Delsanto S, Molinari F, Giusetto P, Liboni W, Badalamenti S, Suri JS: Characterization of a completely user-independent algorithm for carotid artery segmentation in 2-D ultrasound images. IEEE Trans Instrum Meas 56(4):1265–1274, 2007
12. Molinari F, Zeng G, Suri JS: An integrated approach to computer-based automated tracing and its validation for 200 common carotid arterial wall ultrasound images: a new technique. J Ultrasound Med 29:399–418, 2010
13. Molinari F, et al: CAUDLES-EF: carotid automated ultrasound double line extraction system using edge flow. J Digit Imaging, 2011. doi:10.1007/s10278-011-9375-0
14. González RC, Woods RE: Digital Image Processing, 2nd edition. Prentice Hall, Upper Saddle River, 2002
15. Duda RO, Hart PE: Use of the Hough transformation to detect lines and curves in pictures. Commun ACM 15:11–15, 1972
16. Weruaga L, Verdú R, Morales J: Frequency domain formulation of active parametric deformable models. IEEE Trans PAMI 26 (12):1568–1578, 2004
17. Verdú R, Larrey J, Morales J: Frequency implementation of the Euler–Lagrange equations for variational image registration. IEEE Signal Process Lett 15:321–324, 2008
18. Unser M: Splines: a perfect fit for medical imaging. Pro Biomed Opt Imag 225–236, 2002